8 January 2001

PHYSICS LETTERS A

ELSEVIER

Physics Letters A 278 (2001) 286–292

www.elsevier.nl/locate/pla

H_3O^+-dependent morphological change in the electrochemical deposition of iron

Ke-Qin Zhang, Mu Wang *, Ru-Wen Peng, Yuming Xiao, Nai-ben Ming

National Laboratory of Solid State Microstructures and Department of Physics, Nanjing University, Nanjing 210093, China

Received 19 May 2000; received in revised form 17 July 2000; accepted 29 November 2000
Communicated by J. Flouquet

Abstract

By in situ optical microscopy and scanning electron microscopy, we investigate the morphology of the iron electrodeposit grown at different H_3O^+ concentration in the electrolyte. The chemical composition of the electrodeposit is analyzed by X-ray diffraction and Mössbauer spectroscopy. It seems that the morphological transitions observed in this system do not relate to the oxidation/passivation of the metallic deposit during the growth. The possible origin of the dependence of deposit morphology on the H_3O^+ in the electrolyte is discussed.

PACS: 81.15.Pq; 47.54.+r; 47.20.Hw; 92.60.Ek
Keywords: Electrochemical deposition; Pattern formation; Electroconvection

Pattern formation and pattern selection are the important issues of nonequilibrium interfacial growth [1–4]. It is well known that the growth morphology depends on the physico-chemical environment in the vicinity of the growth interface. Physically, it has been demonstrated that the external fields, such as the magnetic field [5] and the convective fluid field [6–11], affect the deposit morphology significantly. It has been shown that when the interbranch electroconvection becomes strong enough, the neighboring branches of the deposit may even 'attract' each other and finally form a network pattern [11]. On the other hand, it has been reported that the change of the growth morphology relates to the change of chemical compositions of the deposit. For example, in the electrochemical deposition of copper it has been found that the morphological transition results from the competition of the formation of copper and cuprous oxide [12]. Besides, the finger-like aggregate has been observed in a thin layer cell containing a nonbinary aqueous electrolyte prepared with cupric sulfate and sodium sulfate, which is expected to associate with a chemical-related effective surface tension at the growing interface [13]. Moreover, acid front originated from the hydrolysis of copper ions during the anode dissolution contributes to the morphological transition in the electrodeposition of copper and zinc [14,15]. In this letter we present the studies on the deposit morphology of iron in relation to the pH value of the electrolyte and try to understand the behind mechanism of this effect.

The electrochemical deposition of $FeSO_4$ was carried out in between two glass plates with two parallel electrodes [11,16]. The cell for the electrodeposition was specially designed that the separation of the up-

* Corresponding author.
E-mail address: muwang@netra.nju.edu.cn (M. Wang).

0375-9601/01/$ – see front matter
PII: S0375-9601(00)00794-5

per and the lower glass plates was independent of the thickness of the electrodes [11]. This was achieved by making the upper glass plate narrower than the separation of the two straight, parallel electrodes and controlling the thickness of the electrolyte by the spacers between the two glass plates. The spacers were made of mica sheet and the thickness was selected as 30 μm in this experiment. The advantage of this design is that the hydrogen bubbles, which are abundant especially in the early stage of electrodeposition from $FeSO_4$ solution, can be released easily from the opening of the upper glass plate and the cathode. If the hydrogen bubbles were not released timely, the deposit branches would be blocked by the bubbles. The straight anode was made of a pure iron wire (99.99%, Goodfellow, UK, ∅0.5 mm). The cathode was made of a graphite rod with a cross-section of 0.5 mm × 0.5 mm. A research optical microscope (Orthoplan-pol, Leitz, Germany) with reflection type of interference contrast device (RICD) was used to monitor the growth of the metal deposit and to map the concentration gradient in front of the growing interface. Analytical grade reagent $FeSO_4$ and deionized water were used to prepare the electrolyte for the experiments. The concentration of $FeSO_4$ solution was 0.5 M and the pH of the non-acidified electrolyte was 3.72. The pH of the electrolyte could be modified by introducing drops of dilute sulfuric acid solution. A constant-voltage power supply was employed and the applied voltage across the electrodes could be selected between 4.0 to 20.0 V. The electrodeposition was carried out at room temperature. The structure and the chemical composition of the iron deposit were further analyzed by X-ray diffraction and Mössbauer spectroscopy.

The morphology of the iron deposit depends on the pH of the electrolyte in the electro-deposition. The deposit is tree-like when the pH of the electrolyte is less than 2.00. When the pH is ranged in between 2.00 and 2.22, it becomes mesh-like. Further increase of the pH of the electrolyte leads to a dense-branching morphology. The typical morphologies of these three kinds are shown in Fig. 1. The transition from the mesh-like pattern to the dense-branching morphology, and the subsequent transition from the dense-branching morphology to the mesh-like pattern and the tree-like pattern have been observed [11,16]. Our previous experiments have confirmed that in the case of electrodeposition in $FeSO_4$ aqueous solution,

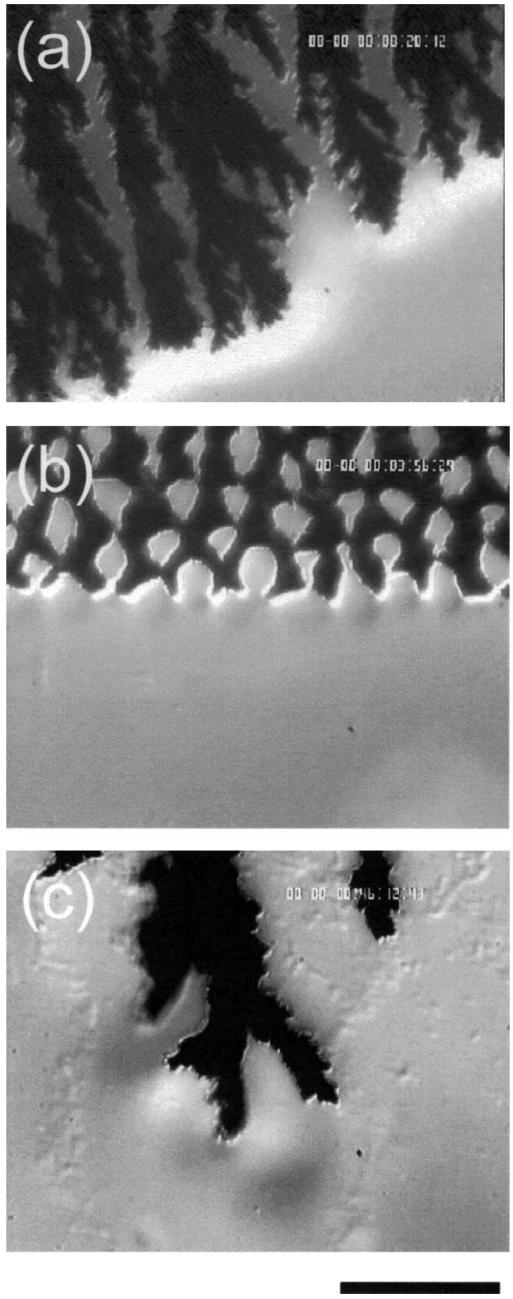

Fig. 1. The typical morphologies during the electrodeposition of iron from $FeSO_4$ aqueous solution (0.5 M), observed by optical interference contrast microscopy. (a) When the initial pH value is above 2.22, the deposit morphology is dense-branching. (b) When pH is in between 2.00 and 2.22, the electrodeposit becomes mesh-like. (c) The tree-like pattern appears when the pH of the electrolyte is less than 2.00. The constant voltage across the electrodes is 8.0 V. The bar represents 100 μm.

the macroscopic morphological transition is related to the interbranch convection, which originates from the presence of H_3O^+ near the growing tips [16].

The microscopic morphology of the deposits is investigated by a scanning electron microscope (SEM) (JSM-6300, JEOL). The samples of the iron deposit are grown at different pH of 3.70, 2.00 and 1.80, respectively, and the corresponding morphologies are dense-branching, mesh-like and tree-like. The deposits are rinsed thoroughly by deionized water to remove the remains of $FeSO_4$ solution. The samples are placed on the glass slides coated with metal film and dried in vacuum before SEM examination. Figs. 2(a) and (a′) show the SEM-view of the deposit of dense-branching morphology. On micrometer scale the deposit is dendritic. Higher magnification shows that the dendritic

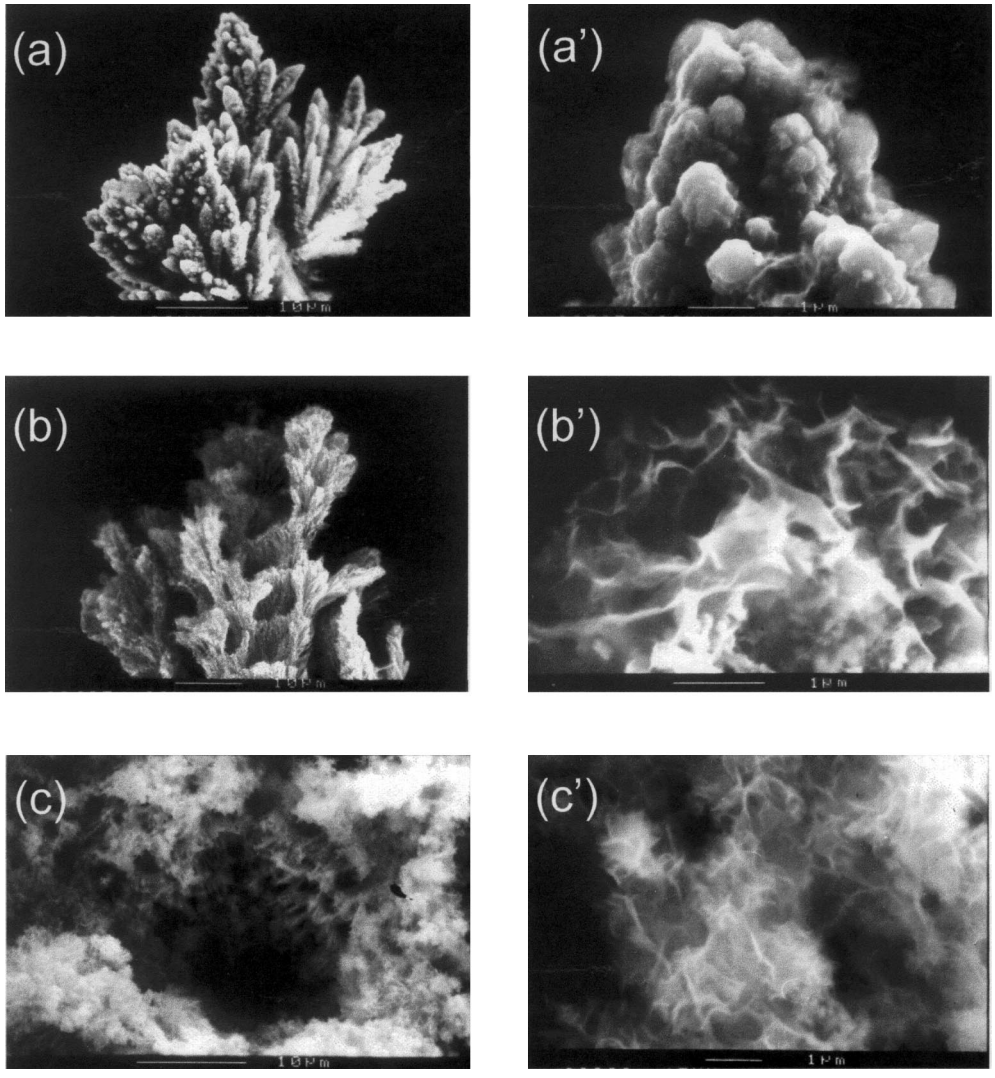

Fig. 2. Scanning electron micrographs of the electrodeposit grown at different pH values. (a) and (a′) show the detailed morphology of the branches of the dense-branching electrodeposit grown at pH = 3.70. (b) and (b′) present the porous surface of the mesh-like deposit grown at pH = 2.00. (c) and (c′) illustrate the surface morphology of the tree-like deposit generated at pH = 1.80.

branches are compact and the surface is roughened (Fig. 2(a′)). Figs. 2(b) and (b′) illustrate the morphology of mesh-like deposit, where porous patterns are revealed. The walls between the random holes and channels are very thin. Figs. 2(c) and (c′) demonstrate the tree-like deposit with high magnification. Similar to that in Figs. 2(b) and (b′), the deposit is porous, however, the size of the holes becomes smaller and the degree of the porosity is clearly increased.

In order to check the chemical composition of the electrodeposits at different growth conditions, we carry out X-ray powder diffraction measurements with Bragg–Brentano $\Theta/2\Theta$ diffractometer (DmaxrB, Rigaku) and CuKα radiation ($\lambda = 1.5418$ Å), at 40 kV and 100 mA. The vacuum-dried deposits grown at different pH values are mounted respectively on silicon single crystalline substrates with (111) orientation. The same amount of the metal deposit is used for the X-ray diffraction for each run. The scan angle is set from 35° to 85° with a step size of 0.02°. The results are shown in Figs. 3(a)–(c). The experimental results are compared with the standard diffraction data. It turns out that in all cases only α-Fe (powder diffraction file (PDF) 6-0696) [17] exists in the samples. No oxide of iron, such as iron trioxide or iron tetroxide have been detected within the accuracy of the X-ray diffractometer. Figs. 3(a)–(c) show that although the positions of the diffraction peaks are the same for the three samples with different morphologies, the intensity of the diffraction peaks varies. The higher diffraction peaks for DBM imply that the grain size and perfection of the crystallization of the dense-branching iron deposit are better than that of the mesh-like and tree-like patterns.

Mössbauer spectroscopy [18,19] is a sensitive method for the phase analysis of the oxidation of iron species. To find out whether trace oxidation has occurred to the metal deposit which is beyond the sensitivity of the X-ray diffraction, a constant acceleration Mössbauer spectrometer with ^{57}Co/Pd source is applied to detect the valence state of iron in the deposit (Fe, Fe^{2+} or Fe^{3+}). The system is calibrated with α-Fe at room temperature before the experiments. The size of the sample cell is $\varnothing 8$ mm $\times$ 0.5 mm. The original experimental data for the deposits grown at different conditions are shown by the dark dots in Fig. 4, which are fitted by curve A. The curve A can be decomposed into two curves B and C by the MOSFUN software, a commonly used Mössbauer spectrum analysis package. It follows that B is a symmetric sextet and C is a doublet. The spectra are characterized by isomer shift (IS) and quadrupole splitting (QS). IS is defined as the shift of the center position of the spectra with respect to the standard spectrum. It originates from the electric monopole (Coulombic) interaction between the nuclear charge distribution over the finite nuclear volume and the electric charge density

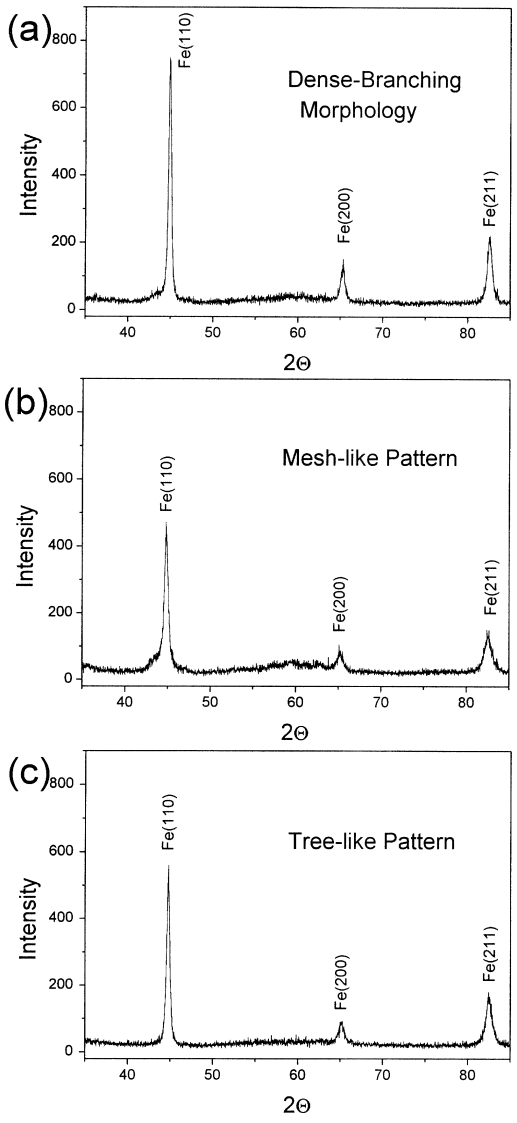

Fig. 3. The X-ray diffraction spectra of the iron deposits with (a) the dense-branching, (b) mesh-like and (c) tree-like morphologies.

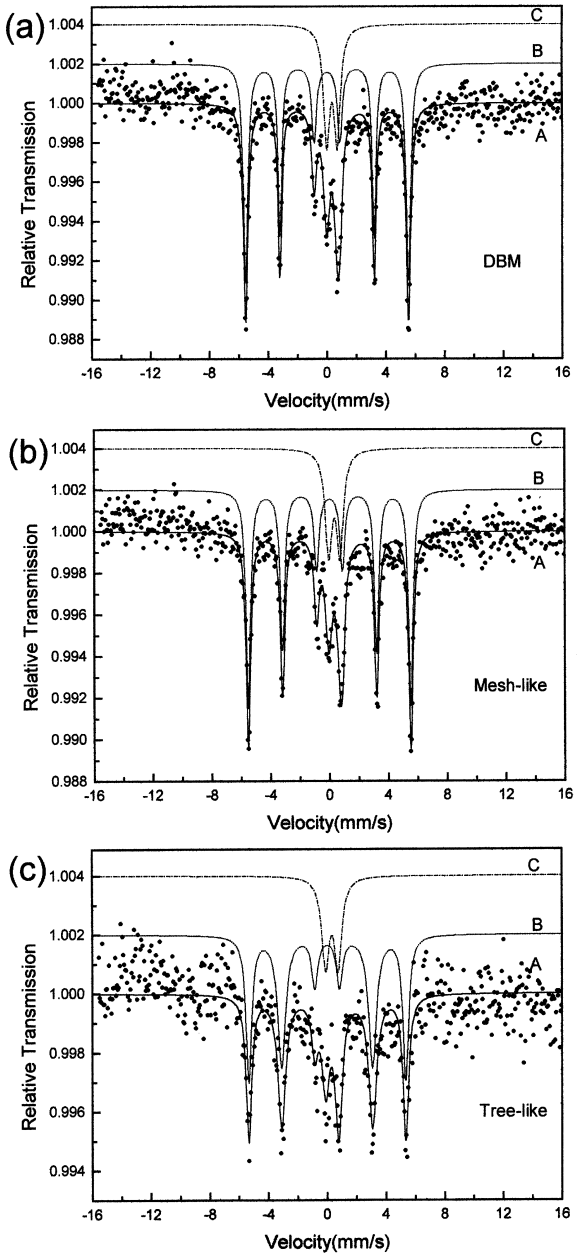

Fig. 4. Mössbauer spectra of the iron deposits grown at different pH values. (a), (b) and (c) correspond to that of the dense-branching morphology, mesh-like pattern and tree-like pattern, respectively.

over this volume. QS is defined as the distance of the doublet of a splitting of the nuclear energy levels. It stands for the interaction between the electric field gradient (EFG) produced by an asymmetric electronic charge distribution and the nuclear quadrupole moment. As shown in Table 1, all the values of IS and QS of spectra B approach zero, suggesting that the samples contain pure metallic iron ^{57}Fe. This result is consistent with that of the X-ray diffraction. For the spectra C of these three samples, the values of IS and QS are listed in Table 1, respectively. According to the literature [19–21], the IS and QS values of superparamagnetic α-Fe_2O_3 and Fe_3O_4 are 0.3, 0.68 and 0.41, 0.02 mm/s, respectively. Whereas FeO is unstable in open air and it easily reacts with oxygen [22]. We also measure the Mössbauer spectrum of analytical pure $FeSO_4$ and the fitting curves indicate IS $\simeq$ 1.26 mm/s and QS $\simeq$ 3.22 mm/s. By comparing these data we conclude that the spectra C are most probably result from the superparamagnetic α-Fe_2O_3 particles in the samples. At this moment, we are not able to judge whether the α-Fe_2O_3 is generated during the electrodeposition process or after the electrodeposition in the open air. It is noteworthy that the line width, the full width at half maximum (FWHM) of the two inner peaks (symmetrical) in spectra B, increases when the pH of the electrolyte increases (Table 1). The FWHM value reflects the long-range order inside the sample [23]. The larger FWHM corresponds to the lower degree of crystallization. Therefore it can be inferred that the degree of crystallization decreases as the concentration of H_3O^+ increases in the electrolyte.

Table 1
Data of Mössbauer spectra

		IS (mm/s)	QS (mm/s)	FWHM (mm/s)
pH = 3.70	B	0.00	0.00	0.39
	C	0.34	0.71	0.51
pH = 2.00	B	0.00	0.00	0.40
	C	0.34	0.77	0.55
pH = 1.80	B	0.01	0.01	0.49
	C	0.32	0.86	0.61
$FeSO_4$		1.26	3.22	0.34
α-Fe_2O_3 [21]		0.300 ± 0.005	0.68 ± 0.01	
Fe_3O_4 [21]		0.41 ± 0.04	0.02 ± 0.04	

It can be seen from Fig. 1 that by increasing the concentration of H_3O^+ the microscopic morphology

of the deposit becomes less ramified on macroscopic scales. One possible reason is the variation of interfacial energy at the growing front for different values of pH of the electrolyte. When the equivalent wetting condition is satisfied, it is known that the surface free energy can be roughly expressed as [24]

$$\gamma = \sum_j \left\{ \frac{1}{2}\left(\phi_j^{AA} - \phi_j^{SS}\right) + X_H^2 \left[\phi_j^{AH} - \frac{1}{2}\left(\phi_j^{AA} + \phi_j^{HH}\right) \right] \right\},$$

where ϕ_j^{AA} stands for the interaction energy of Fe^{2+}–Fe^{2+} in the electrolyte; ϕ_j^{SS} stands for the Fe–Fe interaction energy in the solid electrodeposit; ϕ_j^{AH} for the Fe^{2+}–H_3O^+ interaction energy in the electrolyte; and ϕ_j^{HH} for the H_3O^+–H_3O^+ interaction energy in the electrolyte, respectively. The subscript j covers all the interactions across the solid-liquid interface. X_H denotes the dimensionless concentration of H_3O^+ in the vicinity of the growth front. It follows that the surface free energy is sensitive to the change of pH value in front of the growing interface since it depends on the square of the H_3O^+ concentration. The sign of the second term in the expression of γ is determined by the strength of the interactions ϕ_j^{AA}, ϕ_j^{AH}, and ϕ_j^{HH}, while these terms are the function of the detailed structure and configuration of the corresponding ions in the electrolyte solution. The ramified dense-branching morphology at lower H_3O^+ concentration (Fig. 1(a)) and the ropy pattern at higher H_3O^+ concentration (Figs. 1(b) and (c)) imply that the second term in the surface free energy is positive, i.e., when the concentration of H_3O^+ becomes higher, the surface free energy is increased. As the matter of fact, it has been demonstrated in computer simulations that the growth morphology becomes smoother and more compact when the interfacial energy is taken into account [25,26]. On the other hand, as we pointed out previously, on the macroscopic scale the interbranch electroconvection plays an important role in pattern formation and pattern selection [11,16]. Our observations indicate that the development of the deposit tip depends on the strength and the symmetry of electroconvection on the two sides of the tip. More specifically, the tip splits when the vortices of electroconvection on the two sides of the tip are symmetric. If the electroconvection on the two sides of a tip is apparently asymmetric, which reflects on the contrast around the tip viewed by interference contrast microscopy, the tip will ultimately turn to the neighboring one and a loop will be formed. Therefore, the deposit morphology is modified either by changing the interfacial free energy or by introducing interbranch convection. Both of these two factors relate to the concentration of H_3O^+ in the electrolyte.

It is known that during the electrodeposition of metal, H_3O^+ can be discharged and hydrogen can be absorbed on the metal surface [27,28]. The formation of interstitial hydrogen in copper and copper hydride during hydrogen evolution has been reported in Refs. [29,30]. Similar situation may occur to the electrodeposition of iron. The different amount of hydrogen incorporation at different pH would lead to either different interfacial energy or different interfacial nucleation rate, which may finally contribute to the change of deposit morphologies of the iron. The incorporation of hydrogen in the iron deposit may also be responsible for the porous morphology of the deposit shown in Figs. 2(b), (b′), (c), and (c′). When the concentration of the reduced hydrogen in the electrodeposit becomes sufficiently high, nucleation of H_2 may take place. We suggest that the release of H_2 bubbles from the metal deposit finally leads to the porous morphology.

To summarize, we present here the studies on the morphology of iron electrodeposit at different H_3O^+ concentration in the electrolyte. The experiments show that when the pH of the electrolyte is less than 2.00, the iron electrodeposit is tree-like; when the pH is increased higher than 2.22, the deposit is densely branched; while in between these two values the mesh-like pattern emerges. Our experiments indicate that the change of the deposit morphology is unlikely related to the oxidation of the metal deposit. We suggest that the deposit morphology is affected either by the change of interfacial free energy or the initiation of interbranch convection, both originate from the presence of H_3O^+ at the growing front.

Acknowledgements

We are very grateful to Prof. Yuan-Fu Hsia for stimulating discussion about Mössbauer spectroscopy.

This is work was supported by a grant of the State Key Program for Basic Research from the Ministry of Science and Technology of China and a grant from Natural Science Foundation of China.

References

[1] T. Vicsek, Fractal Growth Phenomena, 2nd ed., World Scientific, Singapore, 1992.
[2] R.M. Brady, R.C. Ball, Nature 309 (1984) 225.
[3] E. Ben-Jacob, P. Garik, Nature (London) 343 (1990) 523.
[4] A.-L. Barabasi, H.E. Stanley, Fractal Concepts in Surface Growth, Cambridge University Press, 1995.
[5] S. Bodca, L. Vignon, R. Ballou, P. Molho, Phys. Rev. Lett. 83 (1999) 2612.
[6] V. Fleury, J.-N. Chazalviel, M. Rosso, Phys. Rev. Lett. 68 (1992) 2492;
V. Fleury, J.-N. Chazalviel, M. Rosso, Phys. Rev. E 48 (1993) 1279.
[7] J.R. de Bruyn, Phys. Rev. Lett. 74 (1995) 4843.
[8] J.M. Huth, H.L. Swinney, W.D. McCormick, A. Kuhn, F. Argoul, Phys. Rev. E 51 (1995) 3444.
[9] D.P. Barkey, D. Watt, Z. Liu, S. Raber, J. Electrochem. Soc. 141 (1994) 1206.
[10] F. Texier, G. Gadret, C. Leger, F. Argoul, J. Phys. II 1 (1997) 663.
[11] M. Wang, W.J.P. van Enckevort, N.-b. Ming, P. Bennema, Nature 367 (1994) 438.
[12] M.-Q. Lopez-Salvans, F. Sagues, J. Claret, J. Bassas, Phys. Rev. E 56 (1997) 6869.
[13] M.-Q. Lopez-Salvans, P.P. Trigueros, S. Vallmitjana, J. Claret, F. Sagues, Phys. Rev. Lett. 76 (1996) 4062.
[14] J.R. Melrose, D.B. Hibbert, R.C. Ball, Phys. Rev. Lett. 65 (1990) 3009.
[15] M.-Q. Lopez-Salvans, F. Sagues, J. Claret, J. Bassas, J. Electroanal. Chem. 421 (1997) 205.
[16] K.-q. Zhang, M. Wang, S. Zhong, G.-X. Chen, N.-B. Ming, Phys. Rev. E 61 (2000) 5512.
[17] Powder diffraction file, 1980. International Center for Diffraction Data, 1601 Park Lane, Swarthmore, PA 19081.
[18] Y. Hsia et al., Mössbauer Effect and Applications, Atomic Energy Press, 1981.
[19] T.C. Gibb, Principles of Mössbauer Spectroscopy, Chapman and Hall, London, 1976.
[20] G.J. Long, F. Grandjean, Mössbauer Spectroscopy Applied to Magnetism and Materials Science, Vol. 1, Plenum Press, New York, 1993.
[21] Y. Hsia, R. Liu, Mössbauer Effect Data Index, Scientific Technique Press, Jiangsu, 1989.
[22] J.C. Bailar et al., Comprehensive Inorganic Chemistry, Vol. 3, Pergamon Press, 1973.
[23] J.A. Dumesic, H. Topsoe, Adv. Catal. 26 (1977) 121.
[24] X.Y. Liu, J. Chem. Phys. 98 (1993) 8154.
[25] T. Vicsek, Phys. Rev. Lett. 53 (1984) 2281.
[26] G. Daccord, J. Nittmann, H.E. Stanley, Phys. Rev. Lett. 56 (1986) 336.
[27] K.N. Srinivasan, M. Selvan, S. Venkata Krishna Iyer, J. Appl. Electrochem. 23 (1993) 358.
[28] B. Bozzini, G. Giovannelli, S. Natali, B. Brevaglieri, P.L. Cavallotti, G. Sigrorelli, Eng. Failure Anal. 6 (1998) 83.
[29] S. Nakahara, Y. Okinaka, Script. Met. 19 (1985) 517.
[30] L. Burzynska, Z. Zembura, J. Karp, React. Solids 7 (1989) 409.